2017-11-30

Mudstones and embedded concretions show differences in lithology-related, but not source-related biomarker distributions

Lengger, SK

10.1016/j.orggeochem.2017.08.003
Organic Geochemistry

Highlights

- Biomarker distributions of concretions and embedding mudstones were similar.
- Only lithology related indices differed between concretions and mudstones.
- Biomarker composition of mud is preserved during concretion formation.
- Biomarker composition of Gogo nodules is related to the palaeoenvironment at time of deposition.

Mudstones and embedded concretions show differences in lithology-related, but not source-related biomarker distributions

Sabine K. Lengger[a,#,*], Ines M. Melendez[a,##] and Kliti Grice[a,*]

a *Western Australian Organic and Isotope Geochemistry Centre, Department of Chemistry, The Institute for Geoscience Research, Curtin University, WA 6102, Bentley, Australia.*

 # Present address: Organic Geochemistry Unit, University of Bristol and The Cabot Institute, Cantock's Close, School of Chemistry, University of Bristol, BS8 1TS, Bristol, UK and University of Plymouth, Biogeochemistry Centre, PL4 8AA, Plymouth, UK.

Present address: Woodside Energy Ltd., Perth, WA, Australia

*corresponding author: k.grice@curtin.edu.au

Abstract

The mudstones of the Western Australian Gogo Formation harbour numerous carbonate concretions which often contain preserved fossils of Lagerstätte-like quality. These are especially notable in places where the mudstone has eroded, giving way to nodule fields, where they are collected for the paleobiological records of great interest they afford. It is, however, a challenge to determine their paleoenvironmental context. Here, we analysed concretions from a core drilled in the Canning Basin Gogo Formation. At two different depths, concretions were compared to the surrounding mudstone found at the same depth. Electron microscopy and X-ray spectroscopy showed that the concretions were carbonate-rich and contained detrital fragments. Biomarker data showed that mudstone and concretions were very similar and presented marine biosignatures including indicators of anoxic depositional conditions, a stratified water column, and photic zone euxinia. The concretions contained higher amounts of C_{27} steranes, indicating that more labile organic matter such as animal remains could have triggered concretion formation. Statistical analyses of the results showed that concretions and shales differed ($p < 0.1$) in indices diagnostic for lithologies (and often related to maturity),

particularly in the sample recovered from the younger section of the core: the diasterane/sterane indices at each of the depths were 0.34 in the shale vs 0.12 in the concretion in the younger, and 0.21 vs 0.19 in the older set of samples. The homohopane isomerisation indices of mudstone and concretion were 0.66 vs 0.58 and 0.62 vs 0.60 (47 and 54 m depth, respectively). Further, shales contained higher relative amounts of moretanes. Concretions also differed from the mudstone in their methylhopane distributions, with shales showing higher amounts of 3-methylhopanes. Conversely, when biomarker composition was compared at the two depths, they only differed significantly ($p < 0.1$) in 2-Methylhopane index, % C_{31} Homohopanes, and hopane/sterane ratios ($p < 0.1$). Our results show that the biomarker composition of the mudstone at the time of deposition is largely preserved in the concretions with only a minor overprint from diagenesis, bacterial communities involved in concretion formation, or the nucleus. It is therefore possible to use biomarker analysis on carbonate concretions to determine their provenance if found outside their immediate geological context.

1. Introduction

The vast stromatoporoid reefs of the Devonian Period (419.2–358.9 Ma) harboured complex and diverse ecosystems, to which formations such as those found in the Canning Basin in the North of Western Australia bear witness (Playford, 1980; Playford et al., 2009). The Gogo Formation is part of this fossil reef complex, and composed of basin facies stemming from the Frasnian to the Givetian. In the Gogo mudstone, the presence of carbonate concretions is notable, and preserved fossils of high quality, close to that of a Lagerstätte, can be found (Long and Trinajstic, 2010). Carbonate concretions have formed diagenetically since the Proterozoic, and are often associated with organic matter-rich sediments (shales, mudstones) and sandstones. It is generally accepted that deposition of organic matter in low oxygen conditions supports their growth and preservation (Berner, 1968; Allison, 1988; Briggs and Kear, 1993; Briggs, 2003; Long and Trinajstic, 2010). They often form as a result of bacterial activity in the anoxic muds, and grow concentrically or pervasively around a centre of decaying organic matter, where microbial sulfate reduction and methanogenesis cause changes in alkalinity (Raiswell and Fisher, 2000). These changes result in fast precipitation of

carbonatesincluding calcite and dolomite, as cements in the pore spaces of unconsolidated sediment, and preservation of the original characteristics of the organic matter nucleus (Wolff et al., 1992). A large number of studies have shown excellent morphological fossil preservation in concretions spanning the entire Phanerozoic (e.g. Weeks, 1953; Marshall and Pirrie, 2013; Wilson and Brett, 2013). Many of these concretions have been eroded out of their embedding rock, are found as large nodules fields in the Canning Basin, and their enclosed fossils, such as the Gogo fish, have afforded major paleobiological insights (Long and Trinajstic, 2010). Biomarker analyses of concretions has shown the preservation of biolipids in very immature stages (Kiriakoulakis et al., 2000; Marynowski et al., 2008; Melendez et al., 2013a, 2013b). Melendez et al. (2013b, 2013a) described the biomarker composition of a soft-tissue concretion from the Gogo Fm. and found exceptionally preserved biomarkers and biomolecules, including a diagenetic continuum of steroids. However, it is poorly understood how the biomarker composition of the Gogo nodules relate to that of the mudstone they are immediately embedded in. A recent comparison of concretions from the Toarcian with their surrounding shale (Posidonia shale, SW German Basin) showed that the biomarker composition of concretions was similar to those of the surrounding shales and thus to environmental conditions at time of formation in those pyritic, organic matter (OM) containing carbonate nodules from this location (Plet et al., 2016). However, this hypothesis requires testing in more settings. Here, we investigated the biomarker compositions of concretions from a core from the Gogo Formation and compared it to the embedding mudstone. The results could allow the use of the biomarker composition to place eroded nodules, such as those found in the North Western Australian nodule fields, in a confirmed paleoenvironmental context.

2. Methods

2.1. Geological setting and core

A core drilled at 18.4818°S 125.9768°E in 1983 by the East Pillara Joint Venture stored at the core repository of the Western Australian Geological Survey (ED20) was examined (Benn and Styles, 1984). It stems from the Canning Basin and was in total 500 m long, of which the upper 110 m

spanned the Gogo Fm. (basin facies of the Givetian to Frasnian; Playford, 1980) consisting of laminated, alternating light and dark grey mudstone with little fauna and of low thermal maturity (Schwark, 2013). At two depths, 47.15–47.45 m, and at 54.56–54.86 m depth, carbonate concretions were found embedded in the mudstones; both were sampled for geochemical analysis. The concretion at 54 m depth was large and partially cored (Fig. S3), whereas the concretion at 47 m depth was a small round nodule of < 10 cm diameter.

2.2 Scanning electron microscopy

The small concretion, taken from the core section at 47 m depth, was cut, polished and coated with Pt using a Cressington 208HR. Scanning electron microscopy and energy-dispersive X-ray spectroscopy imaging was carried out with a Tescan Mira3 FESEM and an Oxford Instruments X-Max 150mm^2 and AZtec software at 15 mm working distance and 20 kV. X-ray diffraction (XRD) patterns of the powdered shales were collected on a D8 Advance diffractometer (Bruker AXS, Germany) using Cu Kα radiation. The data were collected using a 2θ step size of 0.015°, a count time of 0.5 s per step and a 2θ range of 5°–120°. Rietveld modelling with the data was performed using Bruker AXS TOPAS version 5. A corundum (Al_2O_3) internal standard (10 wt.%) was used to facilitate quantitative analysis.

2.3 Extraction, fractionation and derivatisation

The concretions and mudstones were cleaned by 5 x 15 min sonication in dichloromethane /methanol 1:1 (v:v), followed by grinding with a rock grinder using a ceramic bowl that had been baked at 450 °C. The resulting powder was extracted via Soxhlet in dichloromethane (DCM) / methanol (MeOH) 9:1 (v:v) for 72 hours. The extract was concentrated by rotary evaporation and weighed. Aliquots of the total lipid extracts were fractionated by elution over activated silica (SiO_2) with 3 column volumes of hexane (saturate fraction), 3 column volumes of hexane/DCM (7:3, v:v, aromatic fraction) and 3 column volumes of DCM/MeOH (1:1, v:v, polar fraction). For the concretions, the total lipid extract was used after derivatisation with N,O-Bis(trifluoro)acetamide (BSTFA) in pyridine for 1 h at 70 °C. A procedural blank of annealed sand was also processed in the same way. Only a few contaminants,

106 predominantly plasticizers, were identified in the blank. As the focus of this study was to obtain and
107 describe the preserved biomarker fraction rather than determining the fatty acid composition of the
108 concretions, HCl dissolution prior to extraction (Wolff et al., 1992; Pearson et al., 2005) was in this
109 case not employed.

110 *2.4 Biomarker identification*

111 The aromatic fraction of the mudstones, the total lipid extract (TLE) of the concretions and the
112 procedural blank were analysed by gas-chromatography mass spectrometry (GC-MS) as described by
113 Tulipani et al. (2015a) in order to evaluate the carotenoid pigment contents. The saturate fraction of
114 the mudstones and the TLE of the concretions was analysed by gas-chromatography metastable
115 reaction monitoring (GC-MRM) (Tulipani et al., 2015b) in order to determine the sterane and hopane
116 biomarkers and ratios and compared to a Blina oil standard. Some C_{33} 3-methylhopanes were
117 tentatively identified by their retention behaviour according to Summons and Jahnke (1992).
118 Additionally, as the biomarker concentrations in the concretions were low, they were analysed by GC-
119 MRM using a DB-5 MS column, monitoring the transitions *m*/*z* 554 → 134 and *m*/*z* 546 → 134 and
120 compared to Blina oil and oil from the Perth Basin in order to identify carotenoid pigments (French et
121 al., 2015). Biomarker ratios were calculated from the areas of the MRM transition peaks as outlined in
122 Peters et al. (2004). Statistical analysis on biomarker ratios was conducted in R using the FactoMineR
123 package (Le et al., 2008).

124

125 **3 Results and discussion**

126 *3.1. Inorganic Geochemistry*

127 QXRD analyses revealed similar mineralogy of both mudstones, which largely consisted of quartz
128 and Muscovite (22 and 26%, Clay), and contained smaller amounts of brushite, pyrite and orthoclase.
129 Electron microscopy of the concretion found at 47 m showed the heterogeneous structure of the
130 concretion (Fig. 1). Elemental mapping confirmed that the main cement of the concretions was
131 $CaCO_3$ (Fig. 1B, Site 1), with fragments of SiO_2 (Fig. 1B, Site 2) and other silicates (Fig. 1B, Site 3)

such as K-Feldspar (Fig. 1B, Site 4) and pyrite (Fig. 1B, Site 5). Maps of individual elements of an area containing a small vein (Fig. 1C) confirmed that it consisted of a silicate (Si, Al, O, C, Na, Fig. 1D) and also showed the presence of pyrite (Fe, S, possibly framboidal, Fig. 1D), fragments of apatite (P, Fig. 1D) and albite (Na, Fig. 1D). No obvious preserved fossils or OM-rich areas were detected, suggesting that the concretions were formed around a very small organic nucleus, or that the nucleus had been completely replaced. The lithified carbonate in concretions stems from micro-environmental changes in pH and Ca or Mg ion concentrations by the microbial community involved in organic matter degradation (Wright and Oren, 2005), while the presence of pyrite is indicative of microbial sulphate reduction (MSR). The silicate fragments are probably detrital (Sugitani et al., 1995), although authigenic K-feldspar in carbonates has been reported previously and its formation attributed to sulfate reduction coupled to anaerobic methane oxidation (Jørgensen, 1981). This could provide an explanation for the appearance of silica-filled cracks (Fig. 1D), which could have formed during compression of the carbonate concretions during burial and filled with authigenic silica by either inorganic or microbially-mediated reactions. However, if these cracks were septarian fractures, these would normally be calcite-filled (Kiriakoulakis et al., 2000), and the features found here could rather present the remains of siliceous spicules of marine hexactinellids odemosponges (Uriz et al., 2003).These results confirm that the samples analysed were indeed post-depositional carbonate concretions.

3.2 Biomarkers and derived indicators

Pristane/phytane ratios were low for all samples, and amounted to 0.43 for the concretions and 0.47 and 0.57 for the mudstone, indicating exceptionally low thermal maturity for material of this age. The aromatic fractions of the mudstones possessed small amounts of paleorenieratene and isorenieratene (Fig. 2AB), and GC-MRM analysis of the TLEs confirmed that they were also present in the concretions (Fig. 2CD), providing evidence for photic zone euxinia during deposition of the sediment (Grice et al., 1996; Sinninghe Damsté et al., 2001; Whiteside and Grice, 2016). All samples displayed a high proportion of C_{29} steranes (Table 1, Fig. 3B, Supplementary. Fig. 1), which is common for marine sediments older than 350yr (Moldowan et al., 1985), and would thus be expected from

159 Devonian reef basin facies such as the Gogo Fm. However, the concretions contained slightly more
160 C_{27} steranes (Fig. 3B) and C_{27} diasteranes, while the mudstones contained more C_{29} steranes,
161 indicating that part of the sterane complement contained in the concretions could stem from decaying
162 animal remains providing labile organic matter acting as a nucleus for concretion formation. C_{27}
163 sterols, such as cholesterol, are typically present in higher abundances in animals. This observation
164 has recently also been made for Toarcian nodules in which the C_{27}/C_{29} sterane ratio was slightly
165 higher for the concretions than for the shales (Plet et al., 2016). Only small amounts of C_{30} steranes
166 (*n*- and *iso*propylcholestane) were detected. C_{30} steranes, though present in higher abundances in e.g.
167 the Cryogenian, have been reported to be scarce in samples from e.g. the Lower Paleozoic
168 (Moldowan, 1984; Rohrssen et al., 2015; Gold et al., 2016). However,they are often present in
169 Devonian settings, albeit sometimes in equally low relative proportions (e.g. Tulipani et al., 2015a).

170 The fractional abundances of all (17α,21β + 17β,21α + 17β,21β) C_{31-35} homohopanes, often used for
171 fingerprinting, were very similar across all samples (Fig. 3A), with significant amounts of C_{35}
172 homohopane, the presence of which is generally associated with sulfidic depositional conditions
173 (Sinninghe Damsté et al., 1989; Peters and Moldowan, 1991; Sinninghe Damsté et al., 1995). The
174 similarity of the homohopane fingerprints between muds and concretions indicates that a bacterial
175 community involved in concretion formation did either not produce extended hopanes different from
176 the bacteria in the muds or overlying water column, or that the bacterial community was the same as
177 in the surrounding sediment, and only activity was enhanced due to a localised high concentration of
178 labile organic matter. . It is possible that preservation of the extended hopanes occurred by
179 incorporation into kerogen, during early diagenesis in the presence of reduced-sulfur compounds
180 (Kohnen et al., 1991; Sinninghe Damsté et al., 1995; Wakeham et al., 1995; Grice et al., 1998).
181 However, due to the small size of the concretions (< 10 cm) as sampled from the core, desulfurisation
182 and hydrogen pyrolysis to analyse the sulfur-bound and kerogen-bound fractions could not be applied.
183 C_{29}/C_{30} hopane ratios were highest in the mudstone at 47 m depth, slightly lower in the corresponding
184 concretion and even lower in both the mudstone and the concretion at 54 m, indicating a possible
185 effect of either production of the C_{29} or preferential degradation of the C_{30} hopane during concretion

formation. All samples showed high gammacerane ratios (5.6–6.9, Table 1), indicating a stratified water column during deposition in agreement with recent studies of the paleoenvironmental conditions during the deposition of the muds of the Gogo Formation (Tulipani et al., 2015b). The ratios of diasteranes over steranes were low across all samples, indicating relatively low thermal maturity (0.12–0.34, Table 1). However, relative amounts of diasteranes were higher in the mudstones than in the concretions. This was expected, as the conversion from steranes to diasteranes is clay-catalysed and slower in carbonates than in mudstones (van Kaam-Peters et al., 1998; Nabbefeld et al., 2010). Hopane-derived maturity parameters such as C_{31-35} 22S/(22S+22R) homohopanes and C_{29}Ts/(C_{29} hopane + C_{29} Ts) did vary between concretions and muds, with the muds showing higher amounts of isomerisation of these compounds. Ts/(Tm+Ts), however did not vary as strongly: itranged from 0.30 to 0.40, which is typical for anoxic marine, comparatively immature sediments. Isomerization indices in sulfur-rich sedimentary environments can sometimes vary between facies, and depend on side chain length (Köster et al., 1997). In agreement with this, 22S/(22S+SSR)were, overall, lower for the C_{31} hopanes (0.4) compared to the C_{32} to C_{35} homohopanes (0.6). Concretions also showed higher relative amounts of ββ C_{30} hopane (0.25 and 0.28 in concretions, vs 0.21 and 0.24 in muds). The hopane/sterane ratio for all samples was between 0.17 and 0.19.

These results strongly suggest that the biomarker composition of the anoxic mud was preserved during concretion formation. Differences in sterane composition could indicate that part of those are derived from sterols from a former organic matter nucleus. Higher diasterane/sterane , 22S/(22S+22R) hopane, and moretane ratios in the mudstone most likely reflect enhanced isomerisatoin in the presence of clays, which are naturally more abundant in mudstones than in the carbonate concretions.

3.3 Methylhopanes

Methylhopanes derive from bacterially produced 2- and 3-methylbacteriohopanepolyols and can thus be useful in the investigation of organic matter sources as well as bacterially mediated processes. MRM analysis of all samples showed abundant methylhopanes (Supplementary. Fig. 2) which were present in the muds and the concretions. The 2-methylhopane index (2α-methyl-17α,21β-C_{31}-hopane

/ (2α-methyl-17α,21β-C_{31}-hopane + 17α,21β-C_{30}-hopane) varied between concretions and muds. Concretions are also showing much lower relative amounts of 3β- over 2α-methylhopanes than the muds (0.43 vs. 3.04 and 0.17 vs. 1.12 at 47 m; and 1.28 vs. 2.01 and 0.48 vs. 0.96 at 54 m; for C_{31} and C_{32} methylhopanes, respectively). While 2-methylhopanes have been considered cyanobacterial biomarkers, it is now clear that a number of different bacteria have the potential to produce their precursors (Welander et al., 2010; Ricci et al., 2014). They are generally considered to be particularly prevalent in dysoxic environments (Dumitrescu and Brassell, 2005) and have been reported to be particularly abundant in cyanobacterial akinetes from nutrient-starved *Nostoc punctiforme* (Doughty et al., 2009). 3-Methylhopanes can be derived from intraaerobic methanotrophs, from acetic acid bacteria, and possibly a range of other sources (Neunlist and Rohmer, 1985; Simonin et al., 1994; Welander and Summons, 2012; Kool et al., 2014) and are generally observed to be elevated in alkaline, lacustrine source rocks (Farrimond et al., 2004). An explanation for the elevated 3-methylhopanes in the mudstones could be preferential preservation. It is also possible, that the anoxic muds were harbouring microorganisms such as *Acetobacter* sp. or *Methylomirabilis oxyfera* (Ettwig et al., 2010), who produce 3-methylhopanoids (Zundel and Rohmer, 1985; Kool et al., 2014) during burial, while the comparatively rapid microbial processes of concretion formation were not involving these microorganisms. This further confirms that the concretion formation occurred very quickly after burial.

3.4 *Principal component analysis*

Distinctive features confirmed by principal component analysis (PCA) revealed that the first component PC1 could explain differences between mud and concretions (63.10 %), while the second component could explain differences between different depths (23.90 %). Variables that correlated significantly ($p < 0.1$) with PC1 were partly lithology- and partly source-related ratios (Table 2). The lithology-related indices that showed highest significance in their correlation ($p < 0.1$) were the homohopane isomerisation index $C_{31\text{-}35}$ S/(S+R), the diasterane/sterane ratios, some moretane ratios, and the C_{29}Ts/(C_{29} hopane + C_{29} Ts) ratio. These were all higher in the muds, most probably reflecting the higher clay content of the mudstones which catalysed stereochemical conversions. Previously,

differences in moretane/hopane ratios have been linked to clay contents (French et al., 2012). Other variables that were significantly correlated with PC1, and thus differentiated between concretions and shales were the relative amounts of C_{30}, C_{29} and C_{27} steranes and C_{31}/C_{30} hopanes. As discussed in section 3.3, the higher relative amounts of 3β-methylhopanes in the muds than in the concretions (3β-Me αβ hopanes/2α-Me αβ hopanes) showed strong significance. In turn, variables which differentiated the samples from different depths (PC2) were sterane/hopane ratios, indicating different inputs of organic material or possibly a difference in benthic activity, 2-Methylhopane ratios and % C_{31} homohopanes (Table 2, Supplementary. Fig. 1). Only negligible differences in clay content were present in this core, which is probably the reason for the strong similarities between lithology- or maturity related indicators between the two depths (Table S1). Only further studies including dating and paleoenvironmental studies of the core might allow conclusions about the origin of these differences.

4. Conclusions

Biomarker indices determined from carbonate concretions and their surrounding mudstone in the core showed small differences between muds and concretions in those biomarker ratios that are indicative of clay-catalysed conversions in the muds. The stronger differences in source- or process-related biomarker ratios between the muds and the concretions were their methylhopane distributions, which could be due to preferential preservation, or to differences in bacterial processes during concretion formation compared to bacterial activity during burial of the muds; and their C_{27} sterane abundances, which indicates that the concretion formed around labile organic matter such as animal remains. Generally, characteristic biomarker ratios were very similar between concretions and their surrounding muds. This confirms that the organic geochemistry of the carbonates of concretions found in a geologically less clear setting such as the eroded Gogo nodules can be used to place them in a paleoenvironmental context.

Acknowledgements

The authors thank Roger E. Summons for GC-MRM analysis at Massachusetts Institue of Technology, and Geoff Chidlow for technical support. Grice thanks the Australian Research Council (ARC) for an ARC-DORA grant (Grice: DP130100577), the appointment of SKL as a research associate on this project, and the PhD stipend of IMM. Work at MIT was supported by an award (NNA13AA90A) from the NASA Astrobiology Institute. All authors thank the John de Laeter Centre for access to imaging techniques and XRD and Elaine Miller and William Rickard for assistance. Paul Gates and Chris Arthur are thanked for access to software and Megan Rohrssen for insightful discussions. Alex Holman is thanked for preparing the samples for XRD analyses.

References

Allison, P.A., 1988. The Role of Anoxia in the Decay and Mineralization of Proteinaceous Macro-Fossils. Paleobiology 14, 139–154.

Benn, C.J., Styles, G.R., 1984. East Pillara Joint Venture Portion of 04/48 West Kimberly Mineral Field, Western Australia (No. M 1147/10 A14065). BHP Minerals Division Exploration Department, Perth.

Berner, R.A., 1968. Calcium carbonate concretions formed by the decomposition of organic matter. Science 159, 195–197.

Briggs, D.E.G., 2003. The role of decay and mineralization in the preservation of soft-bodied fossils. Annual Review of Earth and Planetary Sciences 31, 275–301.

Briggs, D.E.G., Kear, A.J., 1993. Fossilization of soft tissue in the laboratory. Science 259, 1439–1442.

Doughty, D.M., Hunter, R.C., Summons, R.E., Newman, D.K., 2009. 2-Methylhopanoids are maximally produced in akinetes of Nostoc punctiforme: geobiological implications. Geobiology 7, 524–532.

290 Dumitrescu, M., Brassell, S.C., 2005. Biogeochemical assessment of sources of organic matter and
291 paleoproductivity during the early Aptian Oceanic Anoxic Event at Shatsky Rise, ODP Leg
292 198. Organic Geochemistry 36, 1002–1022.
293 Ettwig, K.F., Butler, M.K., Le Paslier, D., Pelletier, E., Mangenot, S., Kuypers, M.M.M., Schreiber,
294 F., Dutilh, B.E., Zedelius, J., de Beer, D., Gloerich, J., Wessels, H.J.C.T., van Alen, T.,
295 Luesken, F., Wu, M.L., van de Pas-Schoonen, K.T., Op den Camp, H.J.M., Janssen-Megens,
296 E.M., Francoijs, K.-J., Stunnenberg, H., Weissenbach, J., Jetten, M.S.M., Strous, M., 2010.
297 Nitrite-driven anaerobic methane oxidation by oxygenic bacteria. Nature 464, 543–548.
298 Farrimond, P., Talbot, H.M., Watson, D.F., Schulz, L.K., Wilhelms, A., 2004. Methylhopanoids:
299 Molecular indicators of ancient bacteria and a petroleum correlation tool. Geochimica et
300 Cosmochimica Acta 68, 3873–3882.
301 French, K.L., Rocher, D., Zumberge, J.E., Summons, R.E., 2015. Assessing the distribution of
302 sedimentary C_{40} carotenoids through time. Geobiology 13, 139–151.
303 French, K.L., Tosca, N.J., Cao, C., Summons, R.E., 2012. Diagenetic and detrital origin of moretane
304 anomalies through the Permian–Triassic boundary. Geochimica et Cosmochimica Acta 84,
305 104–125.
306 Gold, D.A., Grabenstatter, J., de Mendoza, A., Riesgo, A., Ruiz-Trillo, I., Summons, R.E., 2016.
307 Sterol and genomic analyses validate the sponge biomarker hypothesis. Proceedings of the
308 National Academy of Sciences 113, 2684–2689.
309 Grice, K., Schaeffer, P., Schwark, L., Maxwell, J.R., 1996. Molecular indicators of
310 palaeoenvironmental conditions in an immature Permian shale (Kupferschiefer, Lower Rhine
311 Basin, north-west Germany) from free and S-bound lipids. Organic Geochemistry 25, 131–
312 147.
313 Grice, K., Schouten, S., Peters, K.E., Sinninghe Damsté, J.S., 1998. Molecular isotopic
314 characterisation of hydrocarbon biomarkers in Palaeocene–Eocene evaporitic, lacustrine
315 source rocks from the Jianghan Basin, China. Organic Geochemistry 29, 1745–1764.
316 Jørgensen, N.O., 1981. Authigenic K-feldspar in recent submarine gypsum concretions from
317 Denmark. Marine Geology 39, M21–M25.

318 Kiriakoulakis, K., Marshall, J.D., Wolff, G.A., 2000. Biomarkers in a Lower Jurassic concretion from
319 Dorset (UK). Journal of the Geological Society 157, 207–220.
320 Kohnen, M.E. l., Sinninghe Damsté, J.S., Kock-van Dalen, A. c., Jan, W.D.L., 1991. Di- or
321 polysulphide-bound biomarkers in sulphur-rich geomacromolecules as revealed by selective
322 chemolysis. Geochimica et Cosmochimica Acta 55, 1375–1394.
323 Kool, D.M., Talbot, H.M., Rush, D., Ettwig, K., Sinninghe Damsté, J.S., 2014. Rare
324 bacteriohopanepolyols as markers for an autotrophic, intra-aerobic methanotroph.
325 Geochimica et Cosmochimica Acta 136, 114–125.
326 Köster, J., Van Kaam-Peters, H.M.E., Koopmans, M.P., De Leeuw, J.W., Sinninghe Damsté, J.S.,
327 1997. Sulphurisation of homohopanoids: Effects on carbon number distribution, speciation,
328 and 22S22R epimer ratios. Geochimica et Cosmochimica Acta 61, 2431–2452.
329 Le, S., Josse, J., Husson, F., 2008. FactoMineR: An R Package for Multivariate Analysis. Journal of
330 Statistical Software 25, 1–18.
331 Long, J.A., Trinajstic, K., 2010. The Late Devonian Gogo Formation Lägerstatte of Western
332 Australia: Exceptional Early Vertebrate Preservation and Diversity. Annual Review of Earth
333 and Planetary Sciences 38, 255–279.
334 Marshall, J.D., Pirrie, D., 2013. Carbonate concretions-explained. Geology Today 29, 53–62.
335 Marynowski, L., Zatoń, M., Karwowski, Ł., 2008. Early diagenetic conditions during formation of the
336 Callovian (Middle Jurassic) carbonate concretions from Łuków (eastern Poland): evidence
337 from organic geochemistry, pyrite framboid diameters and petrographic study. Neues
338 Jahrbuch für Geologie und Paläontologie - Abhandlungen 247, 191–208.
339 Melendez, I., Grice, K., Schwark, L., 2013a. Exceptional preservation of Palaeozoic steroids in a
340 diagenetic continuum. Scientific Reports 3. doi:10.1038/srep02768
341 Melendez, I., Grice, K., Trinajstic, K., Ladjavardi, M., Greenwood, P., Thompson, K., 2013b.
342 Biomarkers reveal the role of photic zone euxinia in exceptional fossil preservation: An
343 organic geochemical perspective. Geology 41, 123–126.
344 Moldowan, J.M., 1984. C30-steranes, novel markers for marine petroleums and sedimentary rocks.
345 Geochimica et Cosmochimica Acta 48, 2767–2768.

346 Moldowan, J.M., Seifert, W.K., Gallegos, E.J., 1985. Relationship between petroleum composition
347 and depositional environment of petroleum source rocks. AAPG Bulletin 69, 1255–1268.
348 Nabbefeld, B., Grice, K., Schimmelmann, A., Summons, R.E., Troitzsch, U., Twitchett, R.J., 2010. A
349 comparison of thermal maturity parameters between freely extracted hydrocarbons (Bitumen
350 I) and a second extract (Bitumen II) from within the kerogen matrix of Permian and Triassic
351 sedimentary rocks. Organic Geochemistry 41, 78–87.
352 Neunlist, S., Rohmer, M., 1985. Novel hopanoids from the methylotrophic bacteria *Methylococcus*
353 *capsulatus* and *Methylomonas methanica*. Biochemical Journal 231, 635–369.
354 Pearson, M.J., Hendry, J.P., Taylor, C.W., Russell, M.A., 2005. Fatty acids in sparry calcite fracture
355 fills and microsparite cement of septarian diagenetic concretions. Geochimica et
356 Cosmochimica Acta 69, 1773–1786.
357 Peters, K.E., Moldowan, J.M., 1991. Effects of source, thermal maturity, and biodegradation on the
358 distribution and isomerization of homohopanes in petroleum. Organic Geochemistry 17, 47–
359 61.
360 Peters, K.E., Walters, C.C., Moldowan, J.M., 2004. The Biomarker Guide, 2nd ed. Cambridge
361 University Press, Cambridge.
362 Playford, P.E., 1980. Devonian “Great Barrier Reef” of Canning Basin, Western Australia. The
363 American Association of Petroleum Geologists Bulletin 64, 814–840.
364 Playford, P.E., Hocking, R.M., Cockbain, A.E., 2009. Devonian Reef Complexes of the Canning
365 Basin, Western Australia, Geological Survey of Western Australia, Bulletin.
366 Plet, C., Grice, K., Pagès, A., Ruebsam, W., Coolen, M.J.L., Schwark, L., 2016. Microbially-mediated
367 fossil-bearing carbonate concretions and their significance for palaeoenvironmental
368 reconstructions: A multi-proxy organic and inorganic geochemical appraisal. Chemical
369 Geology 426, 95–108.
370 Raiswell, R., Fisher, Q.J., 2000. Mudrock-hosted carbonate concretions: a review of growth
371 mechanisms and their influence on chemical and isotopic composition. Journal of the
372 Geological Society 157, 239–251.

373 Ricci, J.N., Coleman, M.L., Welander, P.V., Sessions, A.L., Summons, R.E., Spear, J.R., Newman,
374 D.K., 2014. Diverse capacity for 2-methylhopanoid production correlates with a specific
375 ecological niche. The ISME Journal 8, 675–684.
376 Rohrssen, M., Gill, B.C., Love, G.D., 2015. Scarcity of the C30 sterane biomarker, 24-n-
377 propylcholestane, in Lower Paleozoic marine paleoenvironments. Organic Geochemistry 80,
378 1–7.
379 Schwark, L., 2013. Exceptional preservation of microbial lipids in Paleozoic to Mesoproterozoic
380 sediments. Geology 41, 287–288.
381 Simonin, P., Tindall, B., Rohmer, M., 1994. Structure elucidation and biosynthesis of 31-
382 methylhopanoids from Acetobacter europaeus. European Journal of Biochemistry 225, 765–
383 771.
384 Sinninghe Damsté, J.S., Rijpstra, W.I.C., De Leeuw, J.W., Schenck, P.., 1989. The occurrence and
385 identification of series of organic sulphur compounds in oils and sediment extracts: II. Their
386 presence in samples from hypersaline and non-hypersaline palaeoenvironments and possible
387 application as source, palaeoenvironmental and maturity indicators. Geochimica et
388 Cosmochimica Acta 53, 1323–1341.
389 Sinninghe Damsté, J.S., Schouten, S., van Duin, A.C.., 2001. Isorenieratene derivatives in sediments:
390 possible controls on their distribution. Geochimica et Cosmochimica Acta 65, 1557–1571.
391 Sinninghe Damsté, J.S., Van Duin, A.C.T., Hollander, D., Kohnen, M.E.L., De Leeuw, J.W., 1995.
392 Early diagenesis of bacteriohopanepolyol derivatives: Formation of fossil homohopanoids.
393 Geochimica et Cosmochimica Acta 59, 5141–5157.
394 Sugitani, K., Sugisake, R., Adachi, M., 1995. Authigenic carbonate concretions and host shales from
395 the Shimanto Belt, southwestern Japan; implications for carbonate precipitation. Journal of
396 Sedimentary Research 65, 531–540.
397 Summons, R.E., Jahnke, L.L., 1992. Hopenes and hopanes methylated in ring-A: correlation of the
398 hopanoids of extant methylotrophic bacteria with their fossil analogues, in: Biomarkers in
399 Sediments and Petroleum. Prentice Hall, Englewood Cliffs, pp. 182–200.

Tulipani, S., Grice, K., Greenwood, P.F., Haines, P.W., Sauer, P.E., Schimmelmann, A., Summons, R.E., Foster, C.B., Böttcher, M.E., Playton, T., Schwark, L., 2015a. Changes of palaeoenvironmental conditions recorded in Late Devonian reef systems from the Canning Basin, Western Australia: A biomarker and stable isotope approach. Gondwana Research 28, 1500–1515.

Tulipani, S., Grice, K., Greenwood, P.F., Schwark, L., Böttcher, M.E., Summons, R.E., Foster, C.B., 2015b. Molecular proxies as indicators of freshwater incursion-driven salinity stratification. Chemical Geology 409, 61–68.

Uriz, M.-J., Turon, X., Becerro, M.A., Agell, G., 2003. Siliceous spicules and skeleton frameworks in sponges: Origin, diversity, ultrastructural patterns, and biological functions. Microscopy Research and Technique 62, 279–299.

van Kaam-Peters, H.M.E., Köster, J., van der Gaast, S.J., Dekker, M., de Leeuw, J.W., Sinninghe Damsté, J.S., 1998. The effect of clay minerals on diasterane/sterane ratios. Geochimica et Cosmochimica Acta 62, 2923–2929.

Wakeham, S.G., Sinninghe Damsté, J.S., Kohnen, M.E.L., De Leeuw, J.W., 1995. Organic sulfur compounds formed during early diagenesis in Black Sea sediments. Geochimica et Cosmochimica Acta 59, 521–533.

Weeks, L.G., 1953. Environment and Mode of Origin and Facies Relationships of Carbonate Concretions in Shales. Journal of Sedimentary Research 23.

Welander, P.V., Coleman, M.L., Sessions, A.L., Summons, R.E., Newman, D.K., 2010. Identification of a methylase required for 2-methylhopanoid production and implications for the interpretation of sedimentary hopanes. Proceedings of the National Academy of Sciences 107, 8537–8542.

Welander, P.V., Summons, R.E., 2012. Discovery, taxonomic distribution, and phenotypic characterization of a gene required for 3-methylhopanoid production. Proceedings of the National Academy of Sciences 109, 12905–12910.

Whiteside, J.H., Grice, K., 2016. Biomarker Records Associated with Mass Extinction Events. Annual Review of Earth and Planetary Sciences 44, 581–612.

Wilson, D.D., Brett, C.E., 2013. Concretions as sources of exceptional preservation, and decay as a source of concretions: Examples from the Middle Devonian of New York. PALAIOS 28, 305–316.

Wolff, G.A., Rukin, N., Marshall, J.D., 1992. Geochemistry of an early diagenetic concretion from the Birchi Bed (L. Lias, W. Dorset, U.K.). Organic Geochemistry 19, 431–444.

Wright, D.T., Oren, A., 2005. Nonphotosynthetic bacteria and the formation of carbonates and evaporites through time. Geomicrobiology Journal 22, 27–53.

Zundel, M., Rohmer, M., 1985. Prokaryotic triterpenoids. 1. 3beta-Methylhopanoids from Acetobacter species and Methylococcus capsulatus. European Journal of Biochemistry 150, 23–27.

439 Table 1. Biomarker ratios for the mudstones and the embedded concretions.
440

Biomarker ratio	Mud 47	Nodule 47	Mud 54	Nodule 54
Pristane/phytane	0.57	0.43	0.47	0.43
% C_{27} steranes	32	44	37	41
% C_{28} steranes	17	17	15	15
% C_{29} steranes	50	39	47	44
$C_{30}/(C_{27}\text{-}C_{30})$	0.03	0.01	0.02	0.02
Diasteranes/steranes	0.34	0.12	0.21	0.19
dia$C_{27}/(C_{27}+C_{28}+C_{29})$	0.32	0.51	0.37	0.41
dia$C_{28}/(C_{27}+C_{28}+C_{29})$	0.19	0.17	0.17	0.16
dia$C_{29}/(C_{27}+C_{28}+C_{29})$	0.49	0.32	0.46	0.43
% C_{31} homohopanes	36	29	28	36
% C_{32} homohopanes	18	22	19	19
% C_{33} homohopanes	24	17	25	21
% C_{34} homohopanes	11	18	15	13
% C_{35} homohopanes	11	14	13	11
C_{29}/C_{30} hopane	0.28	0.25	0.25	0.21
C_{31}/C_{30} hopane	0.22	0.16	0.17	0.16
10xGa/(Ga+C_{30} hopane)	5.63	5.70	6.88	5.82
$C_{31\text{-}35}$ 22S/(22S+22R) homohopanes	0.66	0.58	0.62	0.60
C_{31} 22S/(22S+22R) homohopane	0.37	0.46	0.42	0.44
C_{32} 22S/(22S+22R) homohopane	0.69	0.62	0.64	0.62
C_{33} 22S/(22S+22R) homohopane	0.68	0.57	0.63	0.61
C_{34} 22S/(22S+22R) homohopane	0.67	0.60	0.64	0.62
C_{35} 22S/(22S+22R) homohopane	0.67	0.59	0.65	0.64
C_{29}Ts/(C_{29} hopane + C_{29} Ts)	0.27	0.14	0.25	0.21
Ts/(Tm+Ts)	0.32	0.40	0.36	0.30
ββ/(αβ+βα+ββ) C_{30} hopane	0.21	0.25	0.24	0.28
ββ/(αβ+βα+ββ) C_{31} hopane	0.05	0.05	0.04	0.07
ββ/(αβ+βα+ββ) C_{32} hopane	0.06	0.03	0.06	0.05
Hopanes / steranes	0.19	0.18	0.17	0.19
2-Methylhopane index	0.12	0.30	0.39	0.15
2β-Me αβ C_{31} hopane/2α-Me αβ C_{31} hopane	1.59	1.02	1.75	1.25
2β-Me αβ C_{32} hopane/2α-Me αβ C_{32} hopane	1.53	0.94	1.98	1.10
2β-Me αβ C_{33} hopane/2α-Me αβ C_{33} hopane	1.16	0.96	1.54	0.89
3β-Me αβ C_{31} hopane/2α-Me αβ C_{31} hopane	3.04	0.43	2.01	1.28
3β-Me αβ C_{32} hopane/2α-Me αβ C_{32} hopane	1.12	0.17	0.96	0.48
Moretane / hopane ratios				
βα/(αβ + βα) 2α-Me C_{33} hopane	0.15	0.18	0.38	0.19
βα/(αβ + βα) 2α-Me C_{32} hopane	0.29	0.13	0.24	0.26
βα/(αβ + βα) 2α-Me C_{31} hopane	0.26	0.13	0.25	0.17
βα/(αβ + βα) C_{29} hopane	0.32	0.22	0.28	0.24
βα/(αβ + βα) C_{30} hopane	0.13	0.09	0.12	0.07
βα/(αβ + βα) C_{31} hopane	0.20	0.13	0.19	0.15
βα/(αβ + βα) C_{32} hopane	0.18	0.09	0.14	0.14
βα/(αβ + βα) C_{33} hopane	0.25	0.18	0.21	0.20
βα/(αβ + βα) C_{34} hopane	0.20	0.17	0.19	0.18
βα/(αβ + βα) C_{35} hopane	0.20	0.14	0.18	0.15

441

442

443 Table 2. Correlation coefficients with p-values for the ratios determining the first (PC1, 63.10 % of variability)

444 and second component (PC2, 23.90 % of variability).

Biomarker ratio	Correlation	p-value
PC1 (Mud vs Nodule)		
3β-Me αβ C_{31} hopane/2α-Me αβ C_{31} hopane	0.997	0.003
βα/(αβ + βα) C_{34} hopane	0.988	0.012
% C_{29} steranes	0.988	0.012
3β-Me αβ C_{32} hopane/2α-Me αβ C_{32} hopane	0.986	0.014
βα/(αβ + βα) C_{35} hopane	0.981	0.019
$C_{31\text{-}35}$ 22S/(22S+22R) homohopanes	0.980	0.020
βα/(αβ + βα) C_{29} hopane	0.977	0.023
C_{29}Ts/(C_{29} hopane + C_{29} Ts)	0.975	0.025
βα/(αβ + βα) 2α-Me C_{31} hopane	0.975	0.025
βα/(αβ + βα) C_{31} hopane	0.971	0.029
βα/(αβ + βα) C_{33} hopane	0.955	0.045
Diasteranes/Steranes	0.952	0.048
βα/(αβ + βα) C_{32} hopane	0.940	0.060
% C_{33} homohopanes	0.921	0.079
ββ/(αβ+βα+ββ) C_{32} hopane	0.918	0.082
C_{30}/(C_{27}-C_{30})	0.916	0.084
% C_{32} homohopanes	-0.928	0.072
% C_{27} steranes	-0.992	0.008
PC2 (47 vs 54 m)		
2-Methylhopane index	0.953	0.047
% C_{31} homohopanes	-0.948	0.052
Hopanes / steranes	-0.982	0.018

445

446

447 Figure captions.

448 **Figure 1.** Scanning electron microscopy images of one concretion. A shows a backscatter image, and B shows
449 the elemental mapping results for the different types of mineral seen in the backscatter image. C shows a smaller
450 section backscatter image, and D shows element abundances / K of the section shown in C.

451 **Figure 2.** Chromatograms of TLEs and fractions. A BSTFA-derivatised TLE of the concretion at 47 m, B
452 BSTFA-derivatised TLE of the concretion at 54 m. C Saturates fraction of the mudstone at 47 m, D Saturates
453 fraction of the mudstone at 54 m, E Aromatic fraction of the mudstone at 47 m, F aromatic fraction of the
454 mudstone at 54 m. Inserts in E and F show the extracted ion current at *m*/*z* 134, while inserts in A and B show
455 the GC-MRM results of the TLEs for transitions *m*/*z* 546 → 134 and the peaks identified by comparison to
456 Blina-oil standard.

457 **Figure 3.** Biomarker ratios of the mudstones and concretions. Shown are % of homohopanes (A) and ternary
458 diagram of sterane distributions (B).

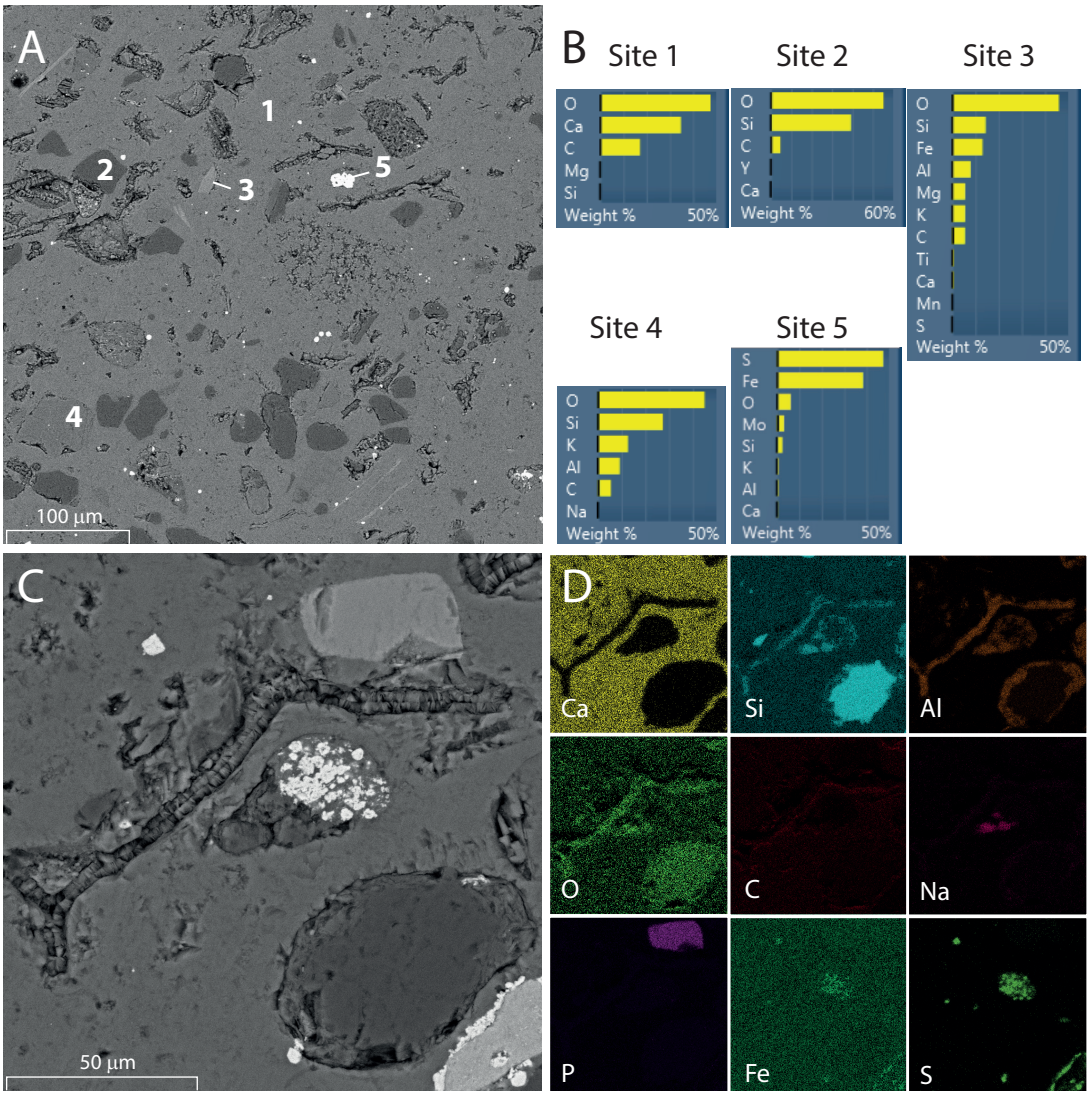
A
1
2
3
4
5
100 µm
B
Site 1
O
Ca
C
Mg
Si
Weight %
50%
Site 2
O
Si
C
Y
Ca
Weight %
60%
Site 3
O
Si
Fe
Al
Mg
K
C
Ti
Ca
Mn
S
Weight %
50%
Site 4
O
Si
K
Al
C
Na
Weight %
50%
Site 5
S
Fe
O
Mo
Si
K
Al
Ca
Weight %
50%
C
50 µm
D
Ca
Si
Al
O
C
Na
P
Fe
S

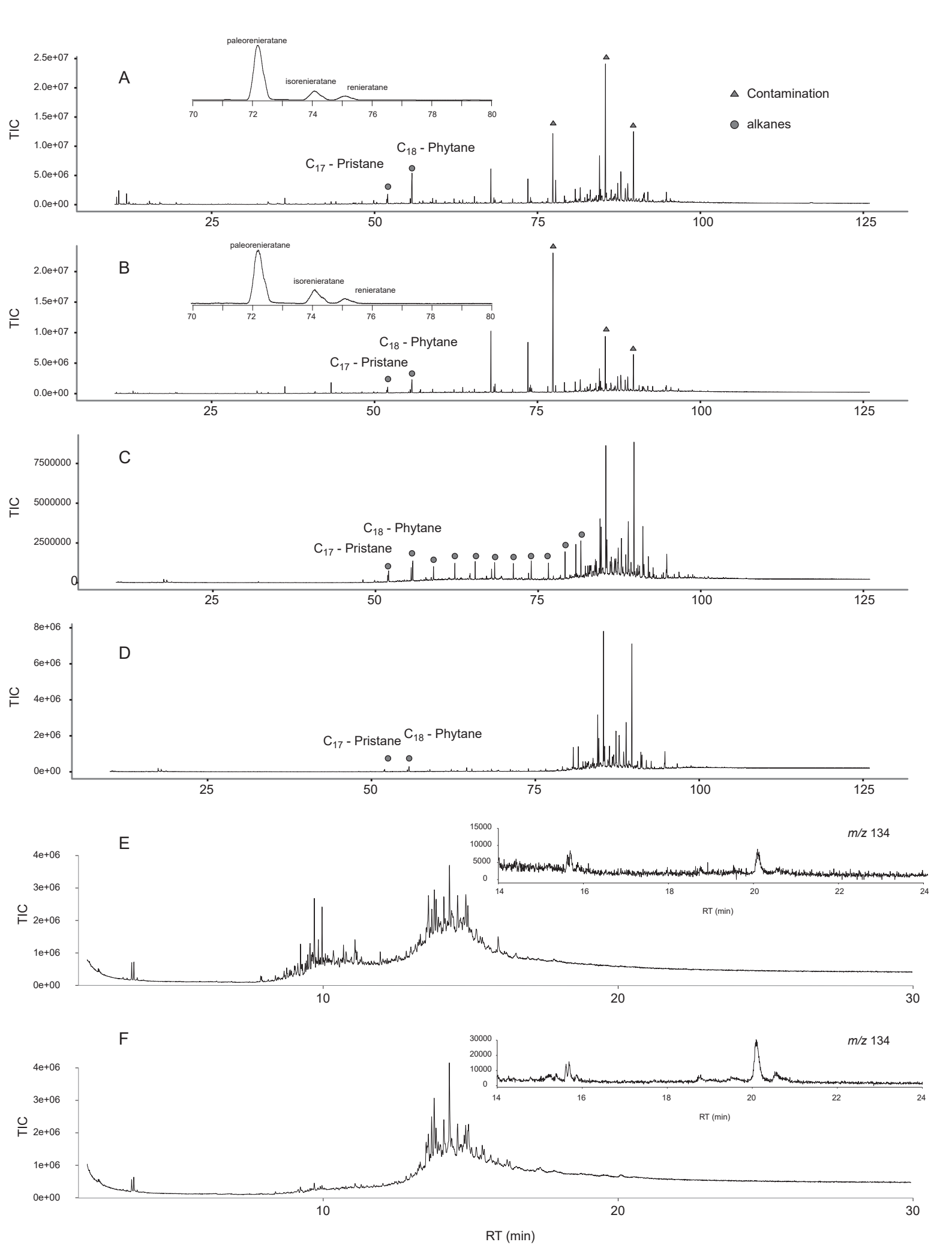
A
B
C
D
E
F
TIC
paleorenieratane
isorenieratane
renieratane
Contamination
alkanes
C17 - Pristane
C18 - Phytane
m/z 134
RT (min)

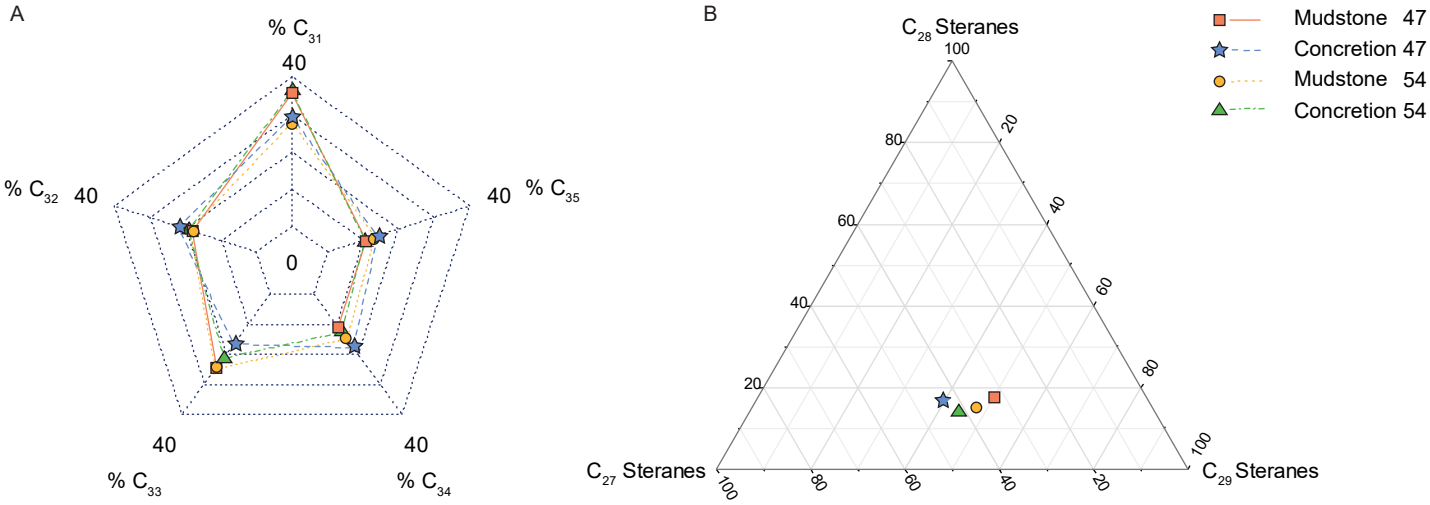
A
% C31
40
% C32
40
0
40
% C35
40
% C33
40
% C34
B
C28 Steranes
100
80
60
40
20
C27 Steranes
100
80
60
40
20
C29 Steranes
100
80
60
40
20
Mudstone 47
Concretion 47
Mudstone 54
Concretion 54

Supplementary Material to *Mudstones and embedded concretions show differences in lithology-related, but not source-related biomarker distributions* by Sabine K. Lengger, Ines M. Melendez, and Kliti Grice.

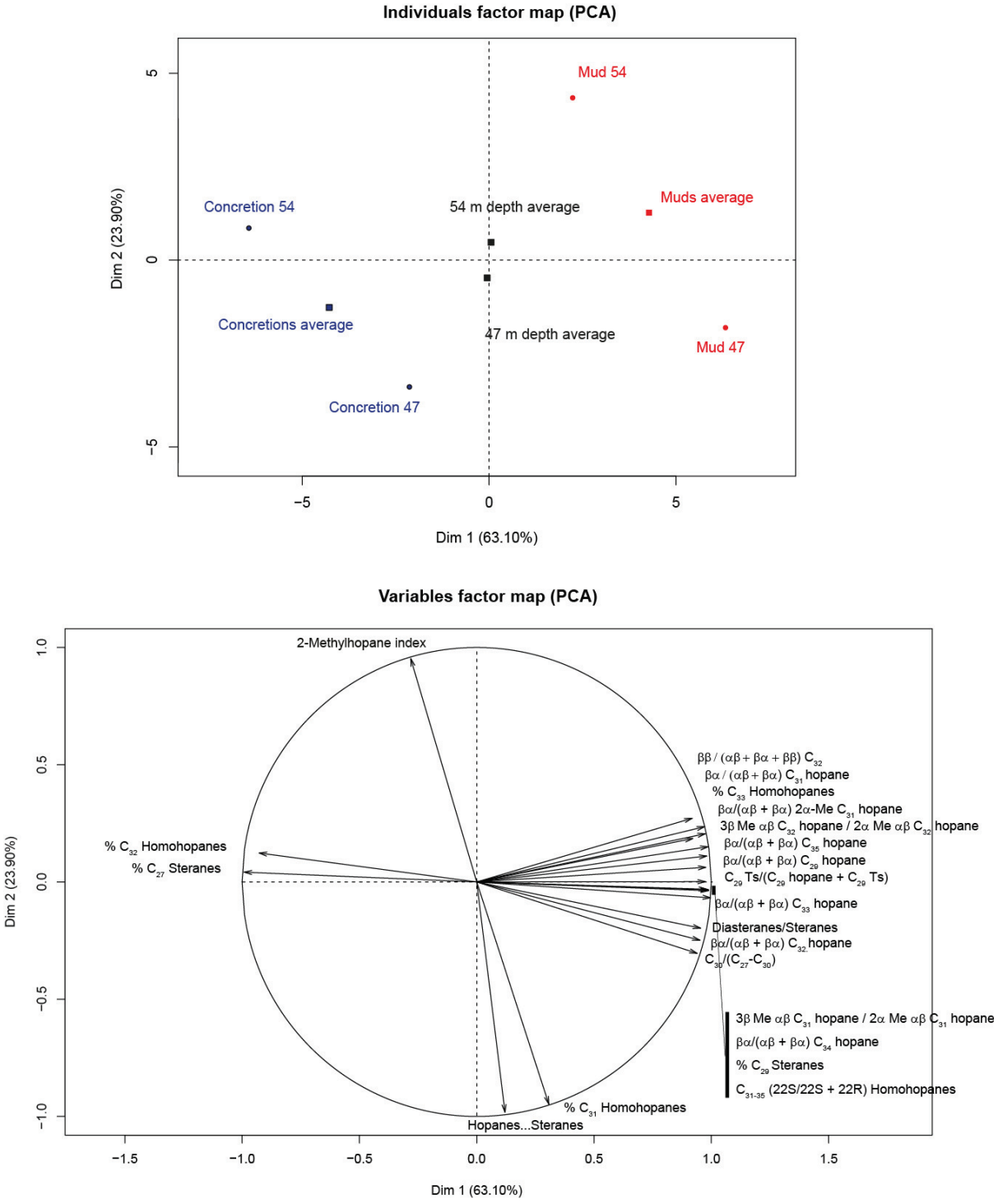

Supplementary Figure 1. Results of the principal component analysis (only significant factors included in the graph).

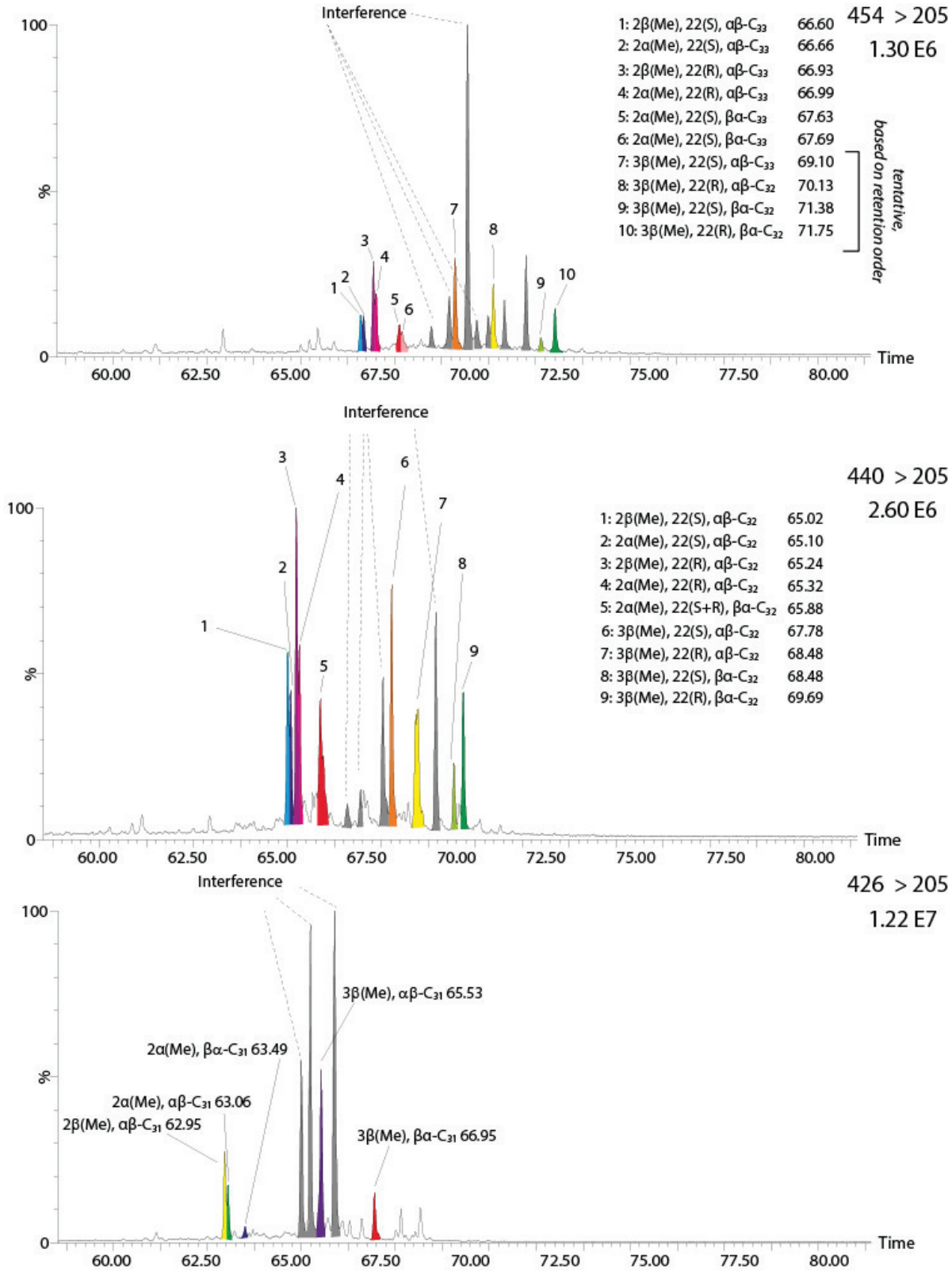

Supplementary Figure 2. Identified methylhopanes.

Supplementary Figure 3. Pictures of the mud and concretion. (A) 47 m depth (concretion), (B) 54 m depth (mudstones and concretion).

Supplementary Table 1. QXRD analysis results

	Quantitative analysis [% w/w]	
	Mudstone 47.15 m	Mudstone 54.46 m
Amorphous content	4.6	6.9
Calcite	1.8	3.0
Pyrite	2.4	2.1
Orthoclase	9.5	10
Muscovite	22	27
Brushite	6.4	6.7
Quartz	53	44